

MOMENTUM CLEANING IN THE CERN LHC

D. Kaltchev, M. Craddock *, R. Servranckx, TRIUMF, Vancouver, Canada
T. Risselada, CERN, Geneva, Switzerland

Abstract

This paper describes the optimization of the optics and of the collimator geometry for the momentum cleaning insertion IR3 of the LHC. To collimate the off-momentum secondary halo without disturbing the circulating beam, the normalized dispersion in IR3 is made as large as in the arcs. The jaw locations and orientations are numerically optimized to reduce the momentum-dependent halo amplitude. The secondary halo is kept within the available aperture for momentum deviations up to 0.44%, where the horizontal aperture is 4σ , compared to 12σ on-momentum.

1 INTRODUCTION

The collimation insertions IR7 and IR3 of the LHC are used for *betatron* and *momentum* cleaning respectively [1]. The latter system must leave the nominal circulating beam unperturbed but be able to intercept off-momentum particles close to the top or bottom of the rf bucket. This requires normalized dispersion in IR3 as large as in the arcs (Sec. 2). The collimators consist of 4 primary and up to 16 secondary pairs of flat jaws. The code DJ (Distribution of Jaws), [2] optimizes the locations and orientations of the collimator jaws in a given lattice with the aim of restricting the maximum extent of the halo generated from the faces of the primary jaws. Only minor modifications to the algorithm of DJ are necessary to describe collimation with $\delta = dp/p \neq 0$, as long as there are no bending magnets between the first primary and last secondary jaws. This is because within this section the “escape polygon” [2] (the window in initial-angle space corresponding to trajectories escaping all secondary collimators), is independent of δ .

2 MOMENTUM CLEANING OPTICS

The *betatron* and *momentum* cleaning insertions of the LHC will use similar magnet configurations. The nominal ring separation is increased locally from 194 to 224 mm using warm dogleg dipoles located at the ends of the long straight sections housing the collimators. All quadrupoles in these straight sections, which have to absorb high levels of particle losses, are normal-conducting. Note that the lattice functions in IR3 and IR7 are quite different: for betatron cleaning the dispersion function D_x and its derivative are tuned to zero at the primary collimators, whereas for momentum cleaning large dispersion values are required.

* Also at Dept. of Physics & Astronomy, UBC, Vancouver, Canada.

The additional requirement that the momentum collimators must never touch the nominal circulating beam points to the “normalized dispersion” $D_x/\sqrt{\beta_x}$ as the quantity to be maximized. If its value at the primary momentum colli-

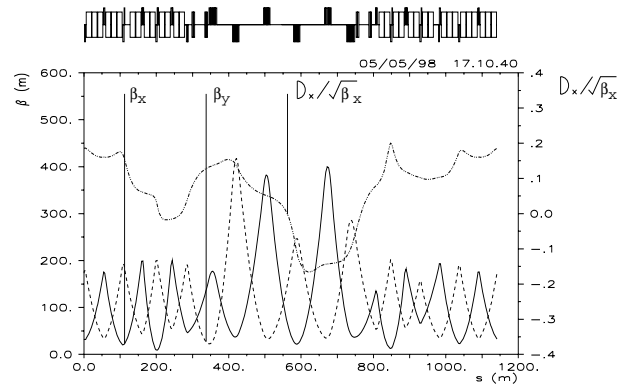


Figure 1: β and normalized dispersion functions in IR3.

mator is large, even off-momentum halo particles close to the nominal beam can be intercepted. Unfortunately the impossibility of changing the machine geometry in the narrow tunnel around IR3 does not allow values larger than in the arcs. In the proposed optics a normalized dispersion close to the arc values is obtained at insertion quadrupole Q5L3. Fig. 1 shows the insertion optics with the beam going from left to right. Figure 2 shows a schematic plot

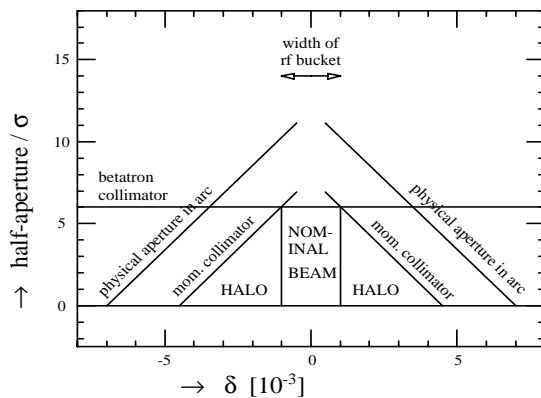


Figure 2: Horizontal - longitudinal shaping of circulating beam and halo by the *primary* betatron and momentum collimators.

of the horizontal mechanical aperture available around the closed orbit for different momentum error values. The plot is made for injection energy conditions and neglects chromatic effects. Only elements with the *smallest* apertures are

shown in the figure, the other elements being in the shadow. The primary collimators are assumed to be flat and upright. For an element with local horizontal orbit distortion x_{co} , rms betatron beam size σ_x , dispersion D_x and mechanical aperture $\pm A_m$ the number of sigmas N_σ available around the closed orbit is given by

$$N_\sigma \sigma_x + |\delta D_x + x_{co}| = A_m$$

Locations with zero dispersion give horizontal lines (e.g. aperture limits in the other insertion straight sections and betatron collimators). Locations with finite dispersion give lines with slope equal to $\pm D_x/\sigma_x$ and thus proportional to their $D_x/\sqrt{\beta_x}$ value. The nominal circulating beam inside the rf buckets and the circulating off-momentum halo are also shown. The latter can circulate with momentum errors as large as $\pm 4.5 \cdot 10^{-3}$.

3 CALCULATION OF THE HALO GEOMETRY

3.1 Halo Definition

The halo is defined and the collimator locations optimized for a single beam passage. When a mono-energetic “ δ -fraction” of the primary (circulating) beam is cut by the primary jaws, scattered particles with the same δ (secondary halo) are generated from each point of the primary jaw faces. Fig. 3 shows a normalized phase-space plot for the scattered particles in a region without bends, but where there is non-zero matched $D_x(s)$. Here s is the longitudinal coordinate; $\eta = D_x/\sqrt{\beta_x \epsilon_x}$ is the normalized dispersion; $\epsilon_x = 7.82 \cdot 10^{-9}$ m.rad is the emittance at injection and the derivative η' is taken with respect to the horizontal phase advance μ_x . In the following, all variables calculated at the point of scatter $P = (x_0, y_0)$ on the primary jaw located at $s = s_0$ have index 0 and we assume that $\mu_x(s_0) = \mu_y(s_0) = 0$. Before the scatter, the turn-by-turn positions of a circulating particle are on the circle (1) centred at $(\delta\eta_0, \delta\eta'_0)$ with radius $A_{x,circ} = |x_0 - \delta\eta_0|$. After scattering (2), the amplitude becomes

$$A_x(x_0, x'_0) = \sqrt{(x_0 - \delta\eta_0)^2 + (x'_0 - \delta\eta'_0)^2}, \quad (1)$$

and the corresponding halo trajectory within the straight is (3), a circle about the origin,

$$x = x_0 \cos \mu_x + x'_0 \sin \mu_x, \quad (2)$$

as is the trajectory of the centre (4).

The secondary halo generated from the source P (x_0, y_0) is then defined to be the set of particle trajectories with initial angles (x'_0, y'_0) , horizontal amplitude (1), and combined (x-y) amplitude

$$A(x_0, x'_0) = \sqrt{(x_0 - \delta\eta_0)^2 + (x'_0 - \delta\eta'_0)^2 + y_0^2 + y'_0{}^2} \quad (3)$$

For a pair (δ, P) to correspond to a halo source, the following two conditions must be simultaneously fulfilled:

1) $|x_0| \geq |\delta\eta_0|$ and 2) x_0 has the same sign as $\delta\eta_0$ (the circle cannot intersect the opposing jaw (Fig. 3, left). Therefore, the one-turn halo is defined for $|\delta| < \delta_{max} \equiv \max_P |x_0|/\eta_0$ ($\eta_0 > 0$).

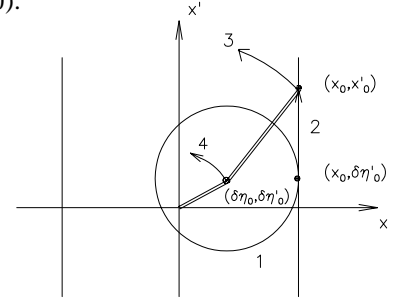


Fig 3, 1 Circulating particle invariant circle. 2 Scattering. 3 Secondary halo trajectory. 4 δ -centre motion.

3.2 Halo computation

The task is, for each δ in the circulating beam, to compute the extent of the halo after collimation, i.e. the maximum amplitudes $A_{x,max}$, $A_{y,max}$, A_{max} surviving all secondary jaws. Rather than scanning over all initial conditions (x_0, y_0, x'_0, y'_0) , DJ uses the mapping technique developed earlier for $\delta = 0$ [2]. For fixed jaw locations, lattice $(\mu_x(s), \mu_y(s), \eta(s))$ and δ , the steps are as follows:

1. A dense set of N_P halo sources, points $P = (x_0, y_0)$, is generated along the primary jaw borders.

2. For each source P :

– using the linear transformation ((2) and a similar one in the y plane) the line boundaries of all secondary jaws are mapped on to the initial-angle plane (x'_0, y'_0) and all intersecting points of the resultant line-images are found;

– among these the program calculates the vertices $(x'_0, y'_0)_i$ ($i = 1, \dots, N_{vert}^{(P)}$) of the “escape polygon”. The amplitudes (1), (3) at the i -th vertex are: $A_{x,i} = A_x(x_0, x'_{0,i})$, $A_i = A(x_0, x'_{0,i})$

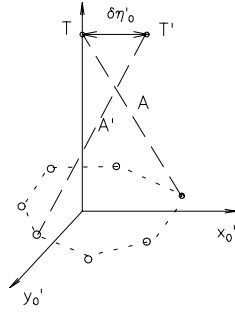
3. The maximum A_i is found by scanning over all $N_{vert}^{(P)} \cdot N_P$ vertices – this is the maximum escaping combined amplitude: $A_{max} = \max_i A_i \equiv A_{i_A}$. The code also stores the corresponding vertex number i_A , source P_A and vertex coordinates (x'_{0,i_A}, y'_{0,i_A}) (maximum surviving scattering angles – see [4] and references there). The same is done for $A_{x,max}$ and $A_{y,max}$.

3.3 δ -dependence of the halo limits. The condition for zero normalized dispersion at the primary collimator.

The set of vertices $(x'_{0,i}, y'_{0,i})$ is independent of δ . It depends only on the lattice and the secondary jaw setup, and represents an escape window in angle space, whose corners move, or may be screened out, as the source P is varied. The corner with index $i = i_A$ determines the maximum escaping amplitude. The δ -dependence of, say, A_{max} comes: 1) explicitly, through the dependence (3) calculated at $(x_0, i_A, x'_{0,i_A}, y_0, i_A, y'_{0,i_A})$ and 2) through the δ dependence of the index i_A .

As δ increases from 0, the maximum vertex i_{A_x} may change many times, or not at all, depending on how η'_0

Fig 4. The escape polygon for fixed P and $A \equiv A_{max}$, the maximum distance (3) from the point T to a vertex. As δ increases, T advances to T', the maximum-vertex number i_A changes, but A_{max} is continuous ($A=A'$). In the limiting case $\eta'_0 = 0$, T remains on the ordinate axis and the maximum vertex is independent of δ .



compares to its critical value $x'_{0,i_{A_x}}/\delta_{max}$. In the limiting case $\eta'_0 = 0$, for a fixed source P, the maximum vertex indices i_A , i_{A_x} and i_{A_y} are independent of δ (Fig. 4). A typical horizontal cutting angle for the IR3 lattice with an optimized setup of 12 to 16 jaws is $3 < |x'_{0,i_{A_x}}| < 4$. A_{max} is a decreasing function of δ (the preferred case for momentum collimation) if $|\eta'_0| < |x'_{0,i_{A_x}}|/\delta_{max} \sim 0.05/\sqrt{\epsilon_x}$.

3.4 Minimization

Minimization in DJ is carried out by the Simulated Annealing (SA) method [3]. For consistent results, the number of sources need not be larger than 20 per primary jaw, which in the case of 4 primary and 16 secondary jaws results in about 3/4 hour native computing time per SA call on `cernsp`. The maximum amplitudes and derivative are taken with appropriate weights in the minimized quantity: $W_1 A_{max}^2 + W_2 A_{x,max}^2 + W_3 (dA_x/d\delta|_{i=i_{A_x}} - A')^2$, normally calculated for δ close to the edge of the bucket. Shaping the function $A_{x,max}(\delta)$ (increasing the slope A' for desired δ) is more effective, but less predictable for $|\eta'_0| > 0.1$. For small $|\eta'_0|$ (~ 0.01), choosing $W_1 = W_2 = 1$, $W_3 = 0$ ensures that the whole curve $A_{x,max}(\delta)$ is shifted downwards.

3.5 Maximum extent of the halo in the arc

At the location in the arc where η reaches its maximum value η_{arc} , the maximum allowed horizontal aperture is $12 \sigma_x$ ($x_{arc} < 12$) [4]. This value follows from geometrical considerations, taking into account vacuum chamber section, maximum horizontal and vertical closed orbit displacements and mechanical alignments. In the arc: $x_{arc} = A_x \cos(\mu_{x,arc} + \mu_0) + \delta \eta_{arc}$. As long as A_x is positive, $x_{arc} \leq A_x + \delta \eta_{arc}$, and it is therefore sufficient to find solutions for which $A_{x,max} < 12 - \delta \eta_{arc}$ for $0 < \delta < \delta_{max}$.

4 RESULTS

Using the lattice of Fig. 1 we install one pair of horizontal primary jaws, each $6.4 \sigma_y$ wide, at maximum normalized dispersion $\eta_0 = 0.153/\sqrt{\epsilon_x}$, ($|\eta'_0| \approx 0$). The jaw aperture chosen (in units of σ) is $n_1 = 7.8$ (making $\delta_{max} = 0.0045$), the smallest possible for betatron collimation primaries set at $n_1 = 6$; thus the line "mom. collimator" in

Fig. 2 just touches the corner of the "nominal beam" rectangle. 16 pairs of secondary jaws are set at $n_2 = 8.8$ and the quantity $A_{x,max}^2 + A_{y,max}^2$ is minimized for $\delta = 0.0045$. Fig. 5 shows the resultant momentum-dependent halo amplitudes: the horizontal amplitude $A_{x,max}$ is seen to be satisfactorily within the $12 - \delta \eta_{arc}$ limit set in the arc focusing quadrupoles (where $\eta_{arc} = 0.16/\sqrt{\epsilon_x}$), for all $\delta < \delta_{max}$. At $\delta = \delta_{max}$ the absolute value of the max-

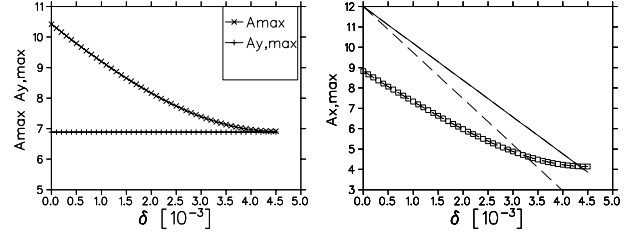


Figure 3: DJ results for the maximum surviving halo amplitudes as a function of δ : (left) vertical and combined; (right) horizontal, with the straight lines showing the $12 - \delta \eta_{arc}$ limits with errors (dashed) and without (solid).

imum cut angle $|x'_{0,i_{A_x}}|$ is 4.07 (not shown) – equal to the theoretical optimum $\sqrt{n_2^2 - n_1^2}$ in the horizontal plane (see [4]). The horizontal amplitude value shown on the plot is $A_{x,max} = 4.14$. This is only a little above the $12 - \delta \eta_{arc}$ limit (3.85). Decreasing the number of secondary jaws from 16 to 6–8 preserves the more important $A_{x,max}$ and leads to an increase of 1-2 σ of A_{max} and $A_{y,max}$. These are generated by a source with $y_0 = 3.2$. For a centred beam, few halo sources are expected that far from the chamber axis, so the effective A_{max} and $A_{y,max}$ are determined by beam position errors at the primary jaw, which have yet to be studied.

The above result concerns an ideal jaw and lattice setup and will be affected by chromatic and misalignment errors. It has been estimated that mismatches in β and D_x [4] could increase the arc η -value from 0.16 up to 0.2 (dashed line). In further simulation runs we therefore allowed a partial cut into the bucket area, allowing $6 < n_1 < 7.8$ (with $n_2 = n_1 + 1$). For the deepest cut $n_1 = 6$ ($\delta_{max} = 0.0035$, $A_{x,max}(\delta_{max}) = 3.6$), but largest errors ($\eta_{arc} = 0.2$), $A_{x,max}$ was well contained within the horizontal aperture and the $A_{max}(\delta = 0)$ was 8.5.

For a larger safety margin, it would be desirable to increase η_0 by around 20%, and this is believed feasible through improvement of the current optical setup.

5 REFERENCES

- [1] The Large Hadron Collider, CERN/AC/95-05(LHC),1995.
- [2] D.I. Kaltchev et al., Proc.EPAC96, (Barcelona, 1996) p. 1432 and CERN LHC Proj.Rep. 37, 1997.
- [3] D.I. Kaltchev et al., Proc.PAC97, (Vancouver, 1997) (in press) and CERN LHC Proj.Rep. 134, 1997.
- [4] J.B.Jeanneret, abs. MOP06C, these proceedings and CERN LHC Proj.Note 115, 1997.